Environmental Sciences Europe

RESEARCH

Open Access

Quantifying photosynthetic performance of phytoplankton based on photosynthesis–irradiance response models

Xiaolong Yang[1], Lihua Liu[2], Zhikai Yin[1], Xingyu Wang[1], Shoubing Wang[1*] and Zipiao Ye[2*]

Abstract

Background: Clarifying the relationship between photosynthesis and irradiance and accurately quantifying photosynthetic performance are of importance to calculate the productivity of phytoplankton, whether in aquatic ecosystems modelling or obtaining more economical production.

Results: The photosynthetic performance of seven phytoplankton species was characterized by four typical photosynthesis–irradiance (*P–I*) response models. However, the differences were found between the returned values to photosynthetic characteristics by different *P–I* models. The saturation irradiance (I_{sat}) was distinctly underestimated by model 1, and the maximum net photosynthetic rate (P_{nmax}) was quite distinct from its measured values, due to the asymptotic function of the model. Models 2 and 3 lost some foundation to photosynthetic mechanisms, that the returned I_{sat} showed significant differences with the measured data. Model 4 for higher plants could reproduce the irradiance response trends of photosynthesis well for all phytoplankton species and obtained close values to the measured data, but the fitting curves exhibited some slight deviations under the low intensity of irradiance. Different phytoplankton species showed differences in photosynthetic productivity and characteristics. *Platymonas subcordiformis* showed larger intrinsic quantum yield (α) and lower I_{sat} and light compensation point (I_c) than *Dunaliella salina* or *Isochrysis galbana*. *Microcystis* sp., especially *M. aeruginosa* with the largest P_{nmax} and α among freshwater phytoplankton strains, exhibited more efficient light use efficiency than two species of green algae.

Conclusions: The present work will be useful both to describe the behavior of different phytoplankton in a quantitative way as well as to evaluate the flexibility and reusability of *P–I* models. Meanwhile we believe this research could provide important insight into the structure changes of phytoplankton communities in the aquatic ecosystems.

Keywords: Phytoplankton, Photosynthetic performance, Irradiance, Photosynthesis–irradiance response model

Background

Phytoplankton are a key functional component of aquatic ecosystems and play a pivotal role in biogeochemical cycles [1]. In particular, marine phytoplankton, as the principal driving force of ocean carbon cycles and energy flows, fix approximately 50 gigatons of inorganic carbon annually, almost half of the total global primary production [2, 3]. They show higher CO_2 fixation rates and higher biomass productivity than any other photosynthetic organisms [3]. As the increase of CO_2 concentration in the atmosphere and global warming, an accurate estimate of photosynthetic productivity of phytoplankton becomes ever more important for modelling primary production and structure changes of phytoplankton communities in aquatic ecosystems, especially eutrophic lakes (e.g., Taihu, Erie, Winnipeg lake) and estuaries (e.g., Yangtze River).

*Correspondence: bswang@fudan.edu.cn; yezp@jgsu.edu.cn
[1] Department of Environmental Science and Engineering, Fudan University, 2005 Songhu Road, Shanghai 200433, People's Republic of China
[2] Institute of Biophysics, Maths & Physics College, Jinggangshan University, 28 Xueyuan Road, Ji'an 343009, People's Republic of China

Clarifying the relationship between photosynthesis and irradiance is a basis to evaluate the growth performance of phytoplankton. Irradiance acts as a driving force in photosynthesis. The level of irradiance affects the growth, CO_2 fixation efficiency, carbon metabolism, and cell composition of photosynthetic organisms [4–8]. High irradiance causes photoinhibition by the production of reactive oxygen species (ROS) and damages the function of the most light-sensitive complex PSII [5]. While extensive studies have been carried out and many insights have enriched the basis of phytoplankton physiology in recent decades [9–11], the relationship remains poorly understood for phytoplankton. Irradiance availability also affects phytoplankton community composition and is one of the key factors causing cyanobacteria blooms [12]. Resource competition theory shows that species with lower "critical light intensity" are often superior, such as *Microcystis* [13].

On the other hand, phytoplankton cells are rich in proteins, polysaccharides, lipids, vitamins, and polyunsaturated fatty acids, which have stirred up great attention as a promising potential feedstock for biofuel, nutraceuticals, animal and aquaculture feed production [10, 14]. Many species have been used for commercial development, such as *Dunaliella salina*, *Isochrysis galbana*, *Spirulina* (or *Arthrospira*), *Haematococcus pluvialis*, and *Scenedesmus obliquus* [2, 6, 10]. Almost all fishes, bivalve molluscs, and crustaceans primarily graze on phytoplankton to build immunity against diseases during their early larval stages [12]. However, large-scale production of phytoplankton has rarely been successful, with no more than 1 g DW L^{-1} biomass that is mainly limited by the inefficiency of photosynthesis in high-cell density cultivation [11, 14, 15]. The photosynthetic parameters can be seen as indicators to achieve sustainable carbon assimilation and TAG accumulation in *Isochrysis zhangjiangensis* [8]. Therefore, accurately quantifying photosynthetic performance is crucial for more economical integration of production management and operation of industrial-scale phytoplankton culture systems [16].

The response curve of photosynthesis to irradiance (*P–I*) has been frequently used to characterize photosynthetic performance by fitting experimental data (measured as oxygen evolution or carbon uptake) with *P–I* models [17]. Obtained photosynthetic parameters, including the maximum net photosynthetic rate (P_{nmax}), the optimal intensity of irradiance (I_{sat}), and the dark respiration rate (R_d) can be regarded as indicator to evaluate the response of organism to meet environmental changes. In phytoplankton, some classical models describing the *P–I* curves were developed by Webb et al. [18], Platt et al. [19–21] and Eilers and Peeters [22], respectively. Later, some mechanistic models characterizing *P–I* curves with considering the underlying biophysical processes of photosynthesis were mainly used to investigate properties of photosynthetic physiology for phytoplankton [23–28], for example, photoinhibition, photoacclimation and dynamic down-regulation of photosynthesis. However, most of mechanistic models have many parameters and complex relationship between photosynthetic rate and irradiance. Consequently, the most extensive application is still found in those classical models. For example, an examination of the literature overwhelmingly reveals in excess of 1950 papers on the double exponential model proposed by Platt et al. [20]. This is most probably because these classical models are simpler than those new models with many complex parameters and processes, and thus those new models would certainly take many years to be fully adopted. Higher plant and phytoplankton possess similar photosynthetic systems. Recently, Ye et al. developed a mechanistic model for higher plants that parameterizes the core characteristics of photosynthesis to highlight processes, including solar energy absorption of photosynthetic pigment molecules, energy transfer, and electron transport between photosynthetic apparatuses [29]. The model with four parameters is relatively simple, and has been widely applied in rice, wheat, soybean, sunflower and other plants [30, 31].

The objective of this study was to determine the various relationships between the photosynthetic productivity of phytoplankton and irradiance intensity and investigate the reliability of *P–I* models to estimate the photosynthetic performance for phytoplankton. We selected the rather extensive range of phytoplankton, including three isolated from the ocean and four from lakes, to measure their photosynthetic oxygen evolution under different irradiance intensity. Obtained *P–I* data were fitted by using *P–I* model for quantization the photosynthetic performances. The *P–I* model for higher plants developed by Ye et al. (it was represented as model 4 in this study) was first used to compare against three most widely applied models for phytoplankton (them were represented as models 1, 2 and 3 in this study, respectively).

Materials and methods

Phytoplankton cultivation

The three strains of marine phytoplankton (*Isochrysis galbana*, *Dunaliella salina* and *Platymonas subcordiformis*) isolated from East China Seas were grown aseptically in f/2 medium. The four strains of freshwater phytoplankton (*Microcystis aeruginosa* FACHB-905, *Microcystis wesenbergii* FACHB-1112, *Scenedesmus obliquus* FACHB-116 and *Chlorococcum* sp. FACHB-1556) were purchased from the Freshwater Algae Culture Collection (FACHB-collection) of the Institute of Hydrobiology, Chinese Academy of Sciences (Wuhan, China) and cultivated in

BG11 medium. The cultures were illuminated by cool white fluorescent bulbs (60 μmol photons m^{-2} s^{-1}) with a photoperiod of 12 h per day at 26 ± 1 °C.

Measurement of photosynthetic oxygen evolution

After 7 to 10 days of incubation, the photosynthetic oxygen-evolving rate of microalgal cells reaching the exponential growth phase was determined using a bio-oxygen meter (Yaxin-1151, Beijing Yaxinliyi Science and Technology Co., Ltd., China). Eight mL cell suspensions of each strain were exposed to increasing orders of irradiance intensity (0, 25, 50, 100, 150, 200, 300, 400, 500, 600, 800, 1000, and 1200 μmol photons m^{-2} s^{-1}), given by a digital LED light source (YX-11LA, Beijing Yaxinliyi Science and Technology Co., Ltd., China), at 25 ± 1 °C. The meter took reads once every 3 s for 5 min in each irradiance measurement point, during which a linear relationship varying with time in oxygen concentration was obtained. Triplicate samples were prepared and measured for each test. The response of the photosynthetic oxygen-evolving rate to irradiance (P_n–I) was fitted with four P–I models [19–22, 29].

Determination of chlorophyll *a* concentration and cell counts

The cells for photosynthetic oxygen-evolving measurement were collected by centrifugation (5600×g) for 10 min at 4 °C. Chlorophyll *a* (Chl *a*) was extracted from microalgal cells in 90% (v/v) acetone and left overnight at 4 °C in darkness. The extracts were then centrifuged at 3600×g for 10 min. The Chl *a* concentration was determined spectrophotometrically in the supernatant with a SP752 UV–Vis spectrophotometer (Spectrum Instruments, Shanghai, China) according to the method of Jeffrey and Humphrey [32]. One-mL cultures of each strain were taken and preserved in Lugol's iodine solution for counting algal cells by a haemocytometer. Each test was conducted in triplicate.

Model description

Model 1

The light dependence of the net photosynthetic rate (P_n) is expressed as [19]:

$$P_n = P_{nmax}\tanh\left(\frac{\alpha I}{P_{nmax}}\right) - R_d, \quad (1)$$

where P_n (μmol O_2 mg^{-1} Chl *a* h^{-1}) is the chlorophyll *a*-normalized net photosynthetic rate at irradiance I, P_{nmax} (μmol O_2 mg^{-1} Chl *a* h^{-1}) is the light-saturated maximum rate of photosynthesis, α (μmol O_2 mg^{-1} Chl *a* h^{-1}/μmol photons m^{-2} s^{-1}) is the light-limited initial slope of P_n–I curve, and R_d (μmol O_2 mg^{-1} Chl *a* h^{-1}) is the dark respiration rate.

As Eq. (1) is an asymptotic function, the saturation irradiance cannot be directly calculated. Therefore, the saturation irradiance (I_{sat}, μmol photons m^{-2} s^{-1}) is obtained by drawing a line from tangent of the initial slope with the plateau of the P_n–I curve onto the x-coordinate [1]. I_{sat} is calculated by the following calculation formula:

$$I_{sat} = \frac{P_{nmax} - R_d}{\alpha}. \quad (2)$$

But the analytic solution of the light compensation point (I_c, μmol photons m^{-2} s^{-1}) cannot be directly obtained by Eq. (1). In order to obtain I_c, Kok effect [33] must be ignored here, and then I_c can be calculated as [21]:

$$I_c = \frac{R_d}{\alpha}. \quad (3)$$

The photosynthetic quantum efficiency (P_n', μmol O_2 μmol photons $^{-1}$) is calculated as:

$$P_n^{'} = \frac{\alpha}{cosh^2\frac{\alpha I}{P_{nmax}}}. \quad (4)$$

Model 2

The light dependence of P_n is expressed as [20, 21]:

$$P_n = P_s\left[1 - \exp\left(-\frac{\alpha I}{P_s}\right)\right]\exp\left(-\frac{\beta I}{P_s}\right) - R_d, \quad (5)$$

where P_n is the chlorophyll *a*-normalized net photosynthetic rate at irradiance I; α is the light-limited initial slope of P_n–I curve; β is the dimensionless parameter reflecting the photoinhibition process; Without photoinhibition, P_s is the maximum photosynthetic output; P_s is the parameter reflecting the maximum, potential, light-saturated, rate of photosynthesis at $\beta > 0$; and R_d is the dark respiration rate.

The I_{sat} is calculated as:

$$I_{sat} = \frac{P_s}{\alpha}\ln\frac{\alpha + \beta}{\beta}. \quad (6)$$

The P_{nmax} can be calculated as:

$$P_{nmax} = P_s\left(\frac{\alpha}{\alpha + \beta}\right)\left(\frac{\beta}{\alpha + \beta}\right)^{\frac{\beta}{\alpha}} - R_d. \quad (7)$$

However, the analytic solution of I_c cannot be directly obtained by Eq. (5). To obtain I_c, the Kok effect must be ignored here, and then I_c can be calculated as:

$$I_c = \frac{R_d}{\alpha}. \tag{8}$$

The photosynthetic quantum efficiency is calculated as:

$$P_n^{'} = \exp\left(-\frac{\beta I}{P_s}\right)\left\{\alpha \exp\left(-\frac{\alpha I}{P_s}\right) - \beta\left[1 - \exp\left(-\frac{\alpha I}{P_s}\right)\right]\right\}. \tag{9}$$

Model 3

The light dependence of P_n is expressed as [22]:

$$P_n = \frac{I}{\alpha I^2 + \beta I + \gamma} - R_d. \tag{10}$$

Here, P_n is the chlorophyll *a*-normalized net photosynthetic rate at irradiance I; α and β are the fundamental parameters, nondimensional; and R_d is the dark respiration rate. The reciprocal of γ is the light-limited initial slope of P_n–I curve.

I_{sat} is calculated as:

$$I_{sat} = \sqrt{\frac{\gamma}{\alpha}}. \tag{11}$$

P_{nmax} is given by:

$$P_{nmax} = \frac{1}{\beta + 2\sqrt{\alpha\gamma}} - R_d. \tag{12}$$

When $P_n = 0$, I_c is given as follows:

$$I_c = \frac{1 - \beta R_d + \sqrt{(1 - \beta R_d)^2 - 4\alpha\gamma R_d}}{2\alpha R_d}. \tag{13}$$

The photosynthetic quantum efficiency is calculated as:

$$P_n^{'} = \frac{\gamma - \alpha I^2}{\left(\gamma + \beta I + \alpha I^2\right)^2}. \tag{14}$$

Model 4

The light dependence of P_n is expressed as [29]:

$$P_n = \alpha \frac{1 - \beta I}{1 + \gamma I} I - R_d. \tag{15}$$

Here P_n is the chlorophyll *a*-normalized net photosynthetic rate at irradiance I, α is the initial slope of the P_n–I response curve, β and γ are the nondimensional parameters reflecting photoinhibition and light saturation, respectively, and R_d is the dark respiration rate.

I_{sat} is calculated as:

$$I_{sat} = \frac{\sqrt{\frac{(\beta+\gamma)}{\beta}} - 1}{\gamma}. \tag{16}$$

P_{nmax} is obtained by:

$$P_{nmax} = \alpha\left(\frac{\sqrt{\beta + \gamma} - \sqrt{\beta}}{\gamma}\right)^2 - R_d. \tag{17}$$

When $P_n = 0$, I_c is given as follows,

$$I_c = \frac{\alpha - \gamma R_d - \sqrt{(\alpha - \gamma R_d)^2 - 4\alpha\beta R_d}}{2\alpha\beta}. \tag{18}$$

The photosynthetic quantum efficiency is calculated as:

$$P_n^{'} = \alpha \frac{1 - 2\beta I - \beta\gamma I^2}{(1 + \gamma I)^2}. \tag{19}$$

Statistical analysis

P_n–I data were fitted using SPSS version 24.0 using nonlinear, least-squares fitting based on the Levenberg–Marquardt algorithm. Duncan's post hoc tests ($p < 0.05$) were performed to establish differences among fitted results from model 1, model 2, model 3 and model 4. Data were reported as the means and standard errors in the calculations. Goodness of fit of the mathematical models to experimental data was assessed using the adjusted coefficient of determination (R^2). Akaike information criterion (AIC) is a standard to measure the best-fit of statistical models. When sample size (n) is small compared to the number of parameters (i.e., $n/k < 40$), the use of a second order, AIC_c ($= AIC + 2k(k+1)/(n-k-1)$) is recommended [34]. In this paper, AIC_c of each model was calculated because of $n/k = 1$ for model 1, yet $n/k = 0.75$ for models 2, 3 and 4.

Results

Comparison of different *P–I* models of production curves

Applying different values of the fundamental parameters to the model, the differences in the characteristics of production curves among models 2, 3 and 4 were compared, save for model 1, without consideration of light-inhibition at high irradiant intensity. Assuming that the initial slope α was 0.5 (the initial slope of the curve equals the reciprocal of γ in model 3), increasing values of the light-saturated or photoinhibition parameters decreased P_{nmax} of the curve and increased the magnitude of inhibition in three types (Fig. 1b–f), which indicated that they could closely reproduce the trend of the P_n–I curve. However, although P_s is defined as being associated with P_{nmax} in model 2, the given value of P_s was over 30 ~ 125%

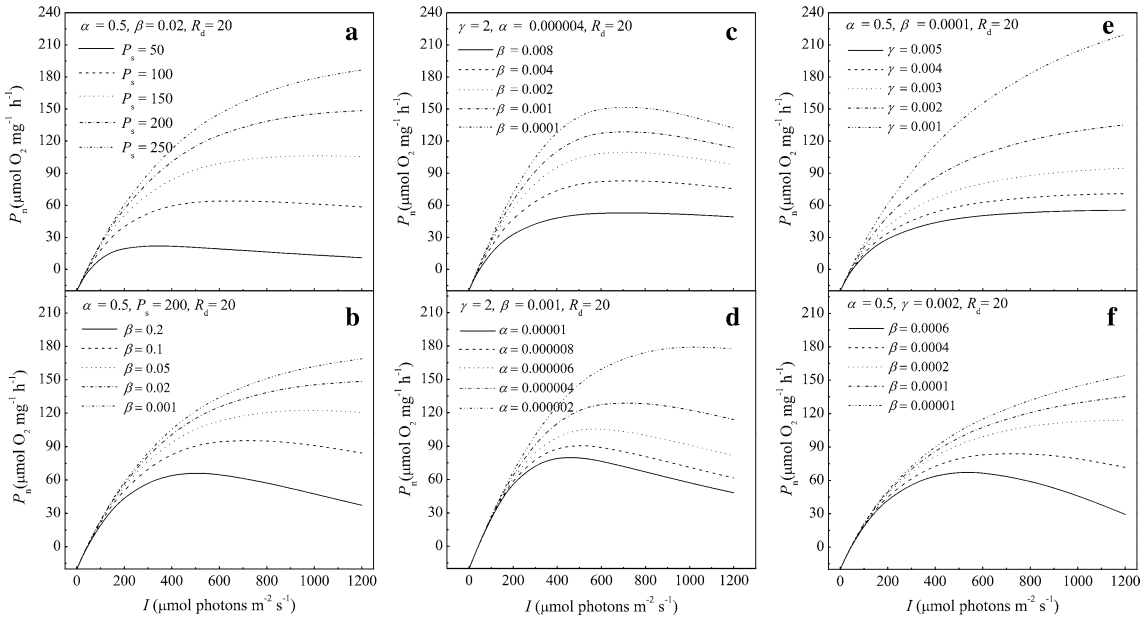

Fig. 1 Models 2, 3 and 4 responses of the net photosynthetic rate (P_n) versus irradiance intensity (I) determined for the different values of the fundamental parameters, respectively. **a**, **b** were obtained by model 2, **c** and **d** were obtained by model 3, and **e** and **f** were obtained by model 4

of P_{nmax}, for which the biological implication is difficult to understand (Fig. 1a). In Fig. 1c, I_{sat} was kept constant value versus the change of β because I_{sat} was barely related to α or γ, according to Eq. 16. And in fact, greater β values were associated with greater bends of the curve, indicating saturation occurred more easily. Thus, Fig. 1c is clearly contradictory to the basis of photosynthetic physiology.

The morphological and growth characteristics of phytoplankter

The morphology of the cultured cells was observed under a 600× optical microscope. Cells were mostly spherical, at 4.3 ~ 10 μm in diameter, and grew singly, except for *S. obliquus*. The Chl *a* contents were 1.647 ± 0.015, 2.778 ± 0.077, 2.297 ± 0.027, 1.320 ± 0.005, 1.739 ± 0.012, 1.318 ± 0.027 and 4.158 ± 0.077 mg L^{-1} for cultures of *I. galbana*, *D. salina*, *P. subcordiformis*, *M. aeruginosa*, *M. wesenbergii*, *S. obliquus* and *Chlorococcum* sp., respectively (Table 1), which was used to normalize the photosynthetic oxygen-producing rate. This normalization will reduce the variability of photosynthetic oxygen-producing rates as a result of differences in biomass, facilitating the comparison of photosynthetic performance. The Chl *a* content per cell of *I. galbana*, *D. salina*, *P. subcordiformis*, *M. aeruginosa*, *M. wesenbergii*, *S. obliquus*, and *Chlorococcum* sp. was 2.570 ± 0.042, 27.118 ± 1.151, 22.931 ± 0.563, 1.972 ± 0.044, 2.404 ± 0.031, 9.126 ± 0.600, and 4.578 ± 0.106 ng 10^4 $cells^{-1}$, respectively.

Table 1 The chlorophyll *a* contents and cell number profiles of seven phytoplankton cultures

Strains	Chl *a* (mg L^{-1})	Cell density (10^4 cells mL^{-1})	Cell size (μm)
I. galbana	1.647 ± 0.015	641.00 ± 5.95	5.8 ± 0.4
D. salina	2.778 ± 0.077	103.00 ± 7.00	9.8 ± 0.2
P. subcordiformis	2.297 ± 0.027	100.33 ± 3.38	10.0 ± 0.1
M. aeruginosa	1.320 ± 0.005	669.67 ± 12.35	4.3 ± 0.4
M. wesenbergii	1.739 ± 0.012	723.33 ± 5.18	5.1 ± 0.2
S. obliquus	1.318 ± 0.027	145.33 ± 6.64	8.1 ± 0.5
Chlorococcum sp.	4.158 ± 0.077	908.67 ± 14.08	6.0 ± 1.2

P_n–I curve and P'_n–I curve of freshwater phytoplankton

The P_n–I curves for *M. aeruginosa*, *M. wesenbergii*, *S. obliquus* and *Chlorococcum* sp. are given in Fig. 2A. For almost all strains, P_n increased rapidly with I under low irradiance intensity, and reached saturation at 400 μmol photons m^{-2} s^{-1}. P_n exhibited a sharp decline for *M. aeruginosa*, *M. wesenbergii*, and *S. obliquus* yet only a slow decline for *Chlorococcum* sp. with the increasing I. The response curves of P_n to I could be divided into three stages in the range of 0 ~ 1200 μmol photons m^{-2} s^{-1}, including photolimitation, photosaturation, and

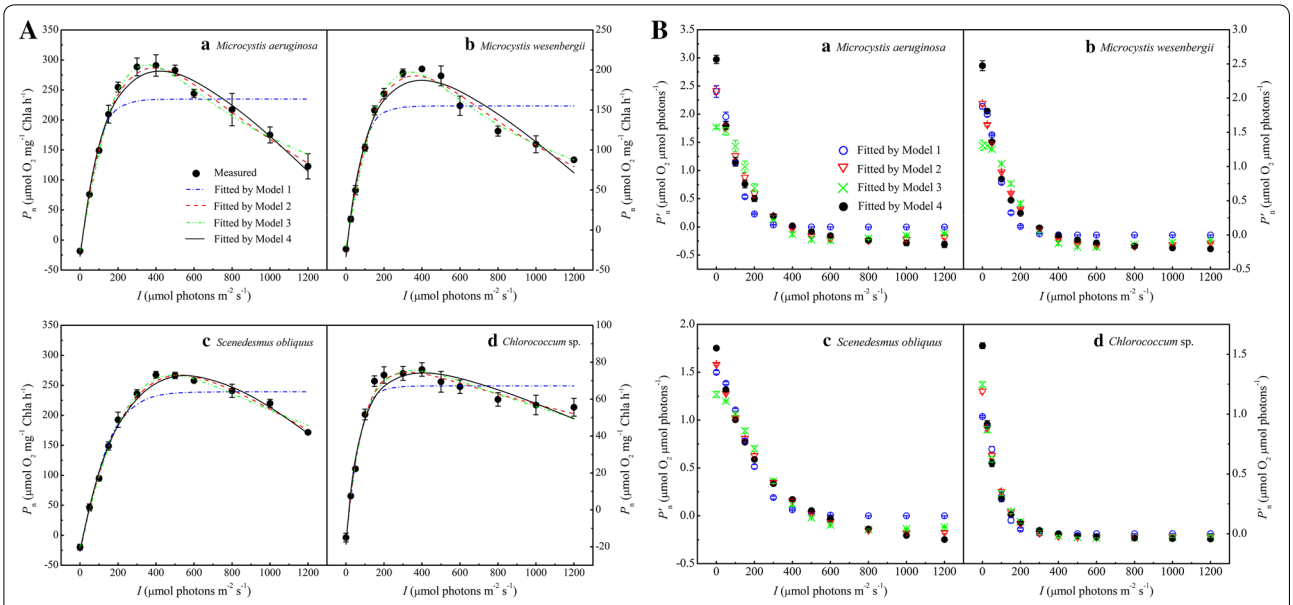

Fig. 2 The P_n–I curves (**A**) and P'_n–I curves (**B**) of *M. aeruginosa*, *M. wesenbergii*, *S. obliquus* and *Chlorococcum* sp

photo-inhibition, by using models 2, 3 and 4, but in addition to those estimated by model 1.

M. aeruginosa and *M. wesenbergii* are two different species of *Microcystis* sp., and despite having nearly identical P_n–I curves, there were some differences in the photosynthetic parameters obtained by the different models (Table 2). The values of P_{nmax} obtained by models 2, 3 and 4 were close to their measured values (approximately 290.83 μmol O_2 mg^{-1} Chl *a* h^{-1} for *M. aeruginosa* and 201.29 μmol O_2 mg^{-1} Chl *a* h^{-1} for *M. wesenbergii*), with < 5% of errors. Nevertheless, the values of I_{sat} calculated by models 2 and 3 for *M. aeruginosa* and *M. wesenbergii* were far below their measured values, with significant differences ($p < 0.05$). For *S. obliquus*, the values of P_{nmax} obtained by models 2, 3 and 4 were just under 1% of the measured value, yet all the corresponding I_{sat} were over the measured value. The P_{nmax} calculated by models 2, 3 and 4 for *Chlorococcum* sp. were 75.25 ± 3.79, 76.15 ± 3.89 and 74.59 ± 4.23 μmol O_2 mg^{-1} Chl *a* h^{-1}, respectively, while the I_{sat} were 311.04 ± 17.27, 339.85 ± 15.19 and 396.06 ± 15.9 μmol photons m^{-2} s^{-1}, respectively. No significant differences were found between the I_{sat} calculated by model 4 and the measured data ($p > 0.05$). The photosynthetic parameters obtained by model 1 were far from the measured data for all strains; above all, the I_{sat} were seriously underestimated. The initial slope of the P_n–I curve α, namely, the intrinsic quantum yield, the estimated by model 4 was the highest for all strains among the other three models. There were no significant differences in the estimation of I_c or R_d among each model.

Figure 2B shows that the quantum yield calculated by models 2, 3 and 4 for *M. aeruginosa*, *M. wesenbergii*, *S. obliquus* and *Chlorococcum* sp. decreased as I increased, until it was equal to zero at the I_{sat} point. Subsequently, it became negative as I increased, which also reveals why P_n decreased as I increased above I_{sat}. However, the values of P'_n obtained by model 1 were always greater than zero with increasing I due to the asymptotic function in this model.

P_n–I curve and P'_n–I curve of marine phytoplankton

The P_n–I curves of *I. galbana*, *D. salina* and *P. subcordiformis* are shown in Fig. 3A, and obvious differences were observed among strains. P_n increased gradually with I towards saturation, which was at 800 μmol photons m^{-2} s^{-1} for *I. galbana*. However, for *D. salina* and *P. subcordiformis*, P_n increased steeply, almost linearly, within low irradiance intensity (below 200 μmol photons m^{-2} s^{-1}), and it decreased rapidly when it reached the maximum value. As was observed for freshwater phytoplankton, all curves stopped above the I_{sat}, excluding those produced by model 1, which indicates the presence of photoinhibition.

Differences were also observed in photosynthetic characteristic parameters calculated by the four types of models (Table 3). Model 1 either overestimated P_{nmax} or underestimated I_{sat}, and these values showed significant differences with their measured values ($p < 0.05$). The P_{nmax} obtained by models 2, 3 and 4 for *I. galbana* were 97.45 ± 3.02, 97.55 ± 3.37 and 98.33 ± 3.20 μmol O_2 mg^{-1} Chl *a* h^{-1}, respectively. The I_{sat} corresponding

Table 2 Comparison of results fitted by models 1, 2, 3 and 4 with measured data in freshwater phytoplankton

Models	Photosynthetic parameters						
	α (μmol O_2 mg^{-1} Chl *a* h^{-1}/ μmol photons m^{-2} s^{-1})	P_{nmax} (μmol O_2 mg^{-1} Chl *a* h^{-1})	I_{sat} (μmol photons m^{-2} s^{-1})	I_c (μmol photons m^{-2} s^{-1})	R_d (μmol O_2 mg^{-1} Chl *a* h^{-1})	R^2	AIC_c
M. aeruginosa							
Model 1	2.404 ± 0.103^{b}	260.46 ± 10.72^{a}	97.83 ± 2.42^{d}	10.57 ± 1.12^{a}	25.63 ± 3.86^{a}	0.721 ± 0.047^{b}	9.270
Model 2	2.416 ± 0.074^{b}	290.74 ± 15.09^{a}	380.17 ± 4.89^{b}	9.47 ± 1.05^{a}	22.92 ± 2.75^{a}	0.973 ± 0.010^{a}	3.772
Model 3	1.770 ± 0.026^{c}	296.37 ± 14.89^{a}	340.82 ± 4.49^{c}	10.26 ± 2.54^{a}	18.23 ± 4.61^{a}	0.969 ± 0.015^{a}	4.687
Model 4	2.967 ± 0.067^{a}	283.55 ± 14.53^{a}	415.25 ± 2.33^{a}	9.53 ± 1.05^{a}	26.86 ± 2.75^{a}	0.964 ± 0.007^{a}	6.783
Measured		≈290.83	≈400	≈10	≈18.27		
M. wesenbergii							
Model 1	1.879 ± 0.039^{b}	184.72 ± 2.57^{c}	82.57 ± 2.56^{d}	15.85 ± 1.68^{a}	29.73 ± 2.91^{ab}	0.758 ± 0.031^{b}	7.329
Model 2	1.920 ± 0.030^{b}	195.32 ± 1.50^{ab}	352.20 ± 7.29^{b}	14.70 ± 1.87^{a}	28.15 ± 2.44^{ab}	0.974 ± 0.006^{a}	4.091
Model 3	1.309 ± 0.074^{c}	201.37 ± 2.94^{a}	322.50 ± 6.96^{c}	15.50 ± 2.37^{a}	20.46 ± 3.90^{b}	0.978 ± 0.007^{a}	2.641
Model 4	2.474 ± 0.071^{a}	188.62 ± 2.31^{bc}	389.62 ± 9.62^{a}	14.81 ± 1.47^{a}	33.19 ± 2.31^{a}	0.954 ± 0.011^{a}	7.327
Measured		≈201.29	≈400	≈15	≈23.73		
S. obliquus							
Model 1	1.499 ± 0.019^{c}	265.88 ± 5.70^{a}	159.64 ± 1.84^{d}	17.82 ± 3.32^{a}	26.61 ± 4.67^{a}	0.912 ± 0.006^{b}	5.606
Model 2	1.581 ± 0.010^{b}	268.80 ± 5.21^{a}	527.39 ± 8.93^{b}	15.24 ± 3.18^{a}	24.05 ± 4.91^{a}	0.989 ± 0.002^{a}	2.757
Model 3	1.268 ± 0.030^{d}	268.70 ± 5.25^{a}	481.60 ± 8.51^{c}	15.34 ± 3.74^{a}	19.25 ± 4.59^{a}	0.989 ± 0.001^{a}	2.607
Model 4	1.751 ± 0.021^{a}	268.11 ± 4.98^{a}	561.94 ± 8.40^{a}	15.82 ± 3.15^{a}	26.29 ± 4.79^{a}	0.987 ± 0.002^{a}	4.077
Measured		≈267.37	≈400	≈15	≈19.91		
Chlorococcum sp.							
Model 1	0.979 ± 0.007^{c}	83.86 ± 4.98^{a}	68.66 ± 4.47^{c}	17.00 ± 1.80^{a}	16.66 ± 1.82^{a}	0.935 ± 0.009^{c}	− 2.268
Model 2	1.190 ± 0.020^{b}	75.25 ± 3.79^{a}	311.04 ± 17.27^{b}	14.59 ± 1.52^{a}	17.43 ± 2.09^{a}	0.984 ± 0.001^{a}	− 1.625
Model 3	1.247 ± 0.022^{b}	76.15 ± 3.89^{a}	339.85 ± 15.19^{b}	15.02 ± 1.76^{a}	16.82 ± 2.09^{a}	0.979 ± 0.002^{ab}	− 0.234
Model 4	1.572 ± 0.024^{a}	74.59 ± 4.23^{a}	396.06 ± 15.93^{a}	13.87 ± 1.59^{a}	18.64 ± 2.18^{a}	0.964 ± 0.001^{b}	1.765
Measured		≈76.06	≈400	≈15	≈15.03		

Different lowercase letters identify groups that are significantly different ($p < 0.05$)

to P_{nmax} were 709.60 ± 26.89, 699.26 ± 32.19, 766.17 ± 24.38 μmol photons m^{-2} s^{-1}, respectively. Despite no significant differences in either estimated P_{nmax} or I_{sat} by the three models ($p > 0.05$), model 4 fitted the values to the measured values with < 5% of errors. For *D. salina*, the P_{nmax} estimated by models 2, 3 and 4 were 113.73 ± 6.24, 114.45 ± 6.24 and 113.31 ± 5.87 μmol O_2 mg^{-1} Chl *a* h^{-1}, respectively, while the I_{sat} obtained by model 2 and model 3 were notably lower than the measured value, with significant differences ($p < 0.05$). The I_{sat} obtained by model 4 was 510.24 ± 2.92 μmol photons m^{-2} s^{-1}, which was quite similar to the measured value (approximately 500 μmol photons m^{-2} s^{-1}). The values of P_{nmax} estimated by models 2, 3 and 4 for *P. subcordiformis* were 94.64 ± 6.65, 95.59 ± 6.63, and 92.20 ± 6.56 μmol O_2 mg^{-1} Chl *a* h^{-1}, respectively; however, the calculated I_{sat} were significantly higher than the measured values ($p < 0.05$), likely because of the rapid increase of P_n during low-intensity irradiance. For α, estimated by model 4 was higher for all strains than those estimated by models 1, 2, and 3, with significant differences ($p < 0.05$) for *D. salina* and *P. subcordiformis*.

The photosynthetic quantum yield represents the efficiency of carbon dioxide fixation or oxygen evolution by a photosynthetic apparatus driven by absorbed photon energy, that is, the conversion efficiency of absorbed solar energy into chemical energy. Figure 3B indicates that the nonlinear change of P'_n as I in three species of marine phytoplankton was similar to that in freshwater phytoplankton.

Discussion

Photosynthesis is not only a biochemical process achieved by photosynthetic apparatuses, it also contains a biophysical process [5, 9, 35]. As shown in Fig. 4, photosynthetic pigment molecules (*Chl*), such as chlorophyll *a* and *b* and carotenoids, absorb solar energy, which induces them into an excited state (*Chl**). The largest amount of exciton binding energy is transferred to

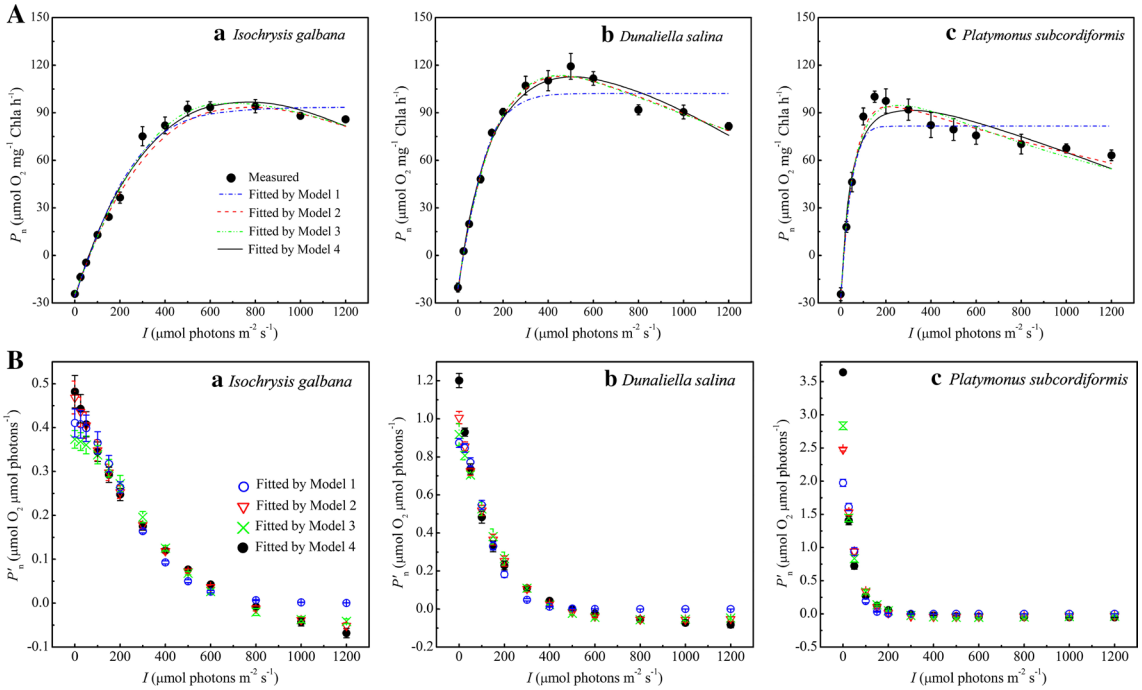

Fig. 3 The P_n–I curves (**A**) and P'_n–I curves (**B**) of *I. galbana*, *D. salina* and *P. subcordiformis*

Table 3 Comparison of results fitted by models 1, 2, 3 and 4 with measured data in marine phytoplankton

Models	Photosynthetic parameters						
	α (μmol O_2 mg^{-1} Chl *a* h^{-1}/ μmol photons m^{-2} s^{-1})	P_{nmax} (μmol O_2 mg^{-1} Chl *a* h^{-1})	I_{sat} (μmol photons m^{-2} s^{-1})	I_c (μmol photons m^{-2} s^{-1})	R_d (μmol O_2 mg^{-1} Chl *a* h^{-1})	R^2	AIC_c
I. galbana							
Model 1	0.411 ± 0.032^{a}	119.51 ± 4.72^{a}	229.90 ± 13.60^{b}	63.12 ± 2.33^{a}	25.97 ± 2.54^{a}	0.981 ± 0.007^{a}	−3.683
Model 2	0.468 ± 0.037^{a}	97.45 ± 3.02^{b}	709.60 ± 26.89^{a}	56.71 ± 2.41^{a}	26.59 ± 2.60^{a}	0.986 ± 0.007^{a}	1.181
Model 3	0.373 ± 0.020^{a}	97.55 ± 3.37^{b}	699.26 ± 32.19^{a}	65.51 ± 3.48^{a}	23.98 ± 1.95^{a}	0.989 ± 0.007^{a}	0.131
Model 4	0.482 ± 0.037^{a}	98.33 ± 3.20^{b}	766.17 ± 24.38^{a}	61.06 ± 2.82^{a}	26.63 ± 2.44^{a}	0.986 ± 0.008^{a}	1.657
Measured		≈94.14	≈800	≈62	≈24.29		
D. salina							
Model 1	0.874 ± 0.023^{c}	123.09 ± 5.88^{a}	116.90 ± 23.87^{c}	23.87 ± 1.66^{a}	20.92 ± 1.97^{a}	0.944 ± 0.016^{b}	0.122
Model 2	1.006 ± 0.033^{b}	113.73 ± 6.24^{a}	453.39 ± 6.87^{b}	21.27 ± 1.75^{a}	21.39 ± 1.81^{a}	0.990 ± 0.001^{a}	−0.018
Model 3	0.918 ± 0.058^{bc}	114.45 ± 6.24^{a}	444.33 ± 6.04^{b}	23.09 ± 2.29^{a}	19.89 ± 1.14^{a}	0.989 ± 0.007^{a}	−0.346
Model 4	1.202 ± 0.037^{a}	113.31 ± 5.87^{a}	510.24 ± 2.92^{a}	21.67 ± 1.93^{a}	23.30 ± 1.93^{a}	0.983 ± 0.002^{a}	1.857
Measured		≈119.24	≈500	≈23	≈20.25		
P. subcordiformis							
Model 1	1.975 ± 0.055^{d}	107.96 ± 5.58^{a}	41.25 ± 1.62^{d}	13.40 ± 2.21^{a}	26.32 ± 3.93^{a}	0.883 ± 0.010^{c}	0.871
Model 2	2.479 ± 0.023^{c}	94.64 ± 6.65^{a}	212.36 ± 7.80^{c}	11.05 ± 1.65^{a}	27.45 ± 4.30^{a}	0.975 ± 0.009^{a}	1.650
Model 3	2.834 ± 0.056^{b}	95.59 ± 6.63^{a}	251.97 ± 9.73^{b}	10.82 ± 1.87^{a}	26.13 ± 4.26^{a}	0.958 ± 0.013^{ab}	3.529
Model 4	3.640 ± 0.031^{a}	92.20 ± 6.56^{a}	299.55 ± 10.72^{a}	9.68 ± 1.71^{a}	28.36 ± 4.21^{a}	0.934 ± 0.013^{b}	5.104
Measured		≈100.13	≈150	≈14	≈24.49		

Different lowercase letters identify groups that are significantly different ($p < 0.05$)

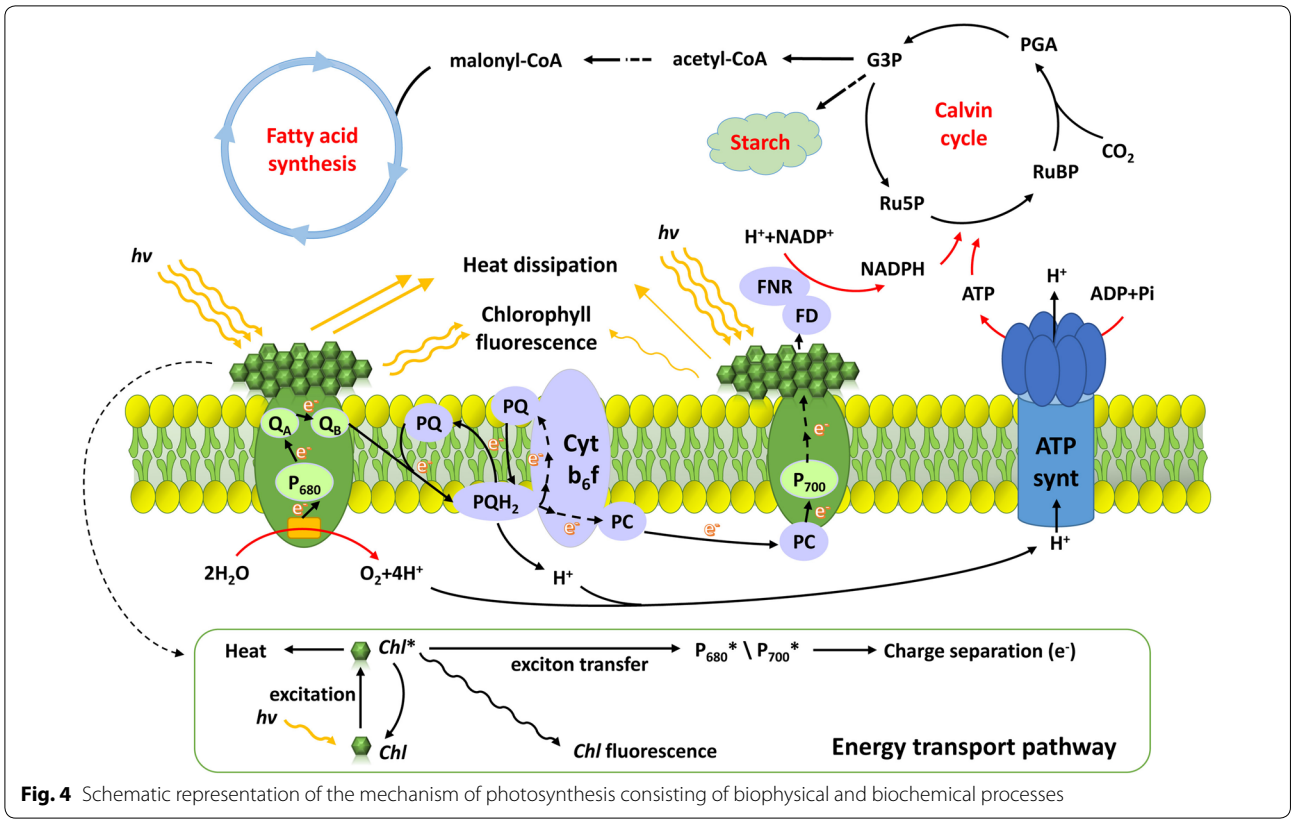

Fig. 4 Schematic representation of the mechanism of photosynthesis consisting of biophysical and biochemical processes

the photochemical reaction centres (e.g., P_{680} and P_{700}), where charge separation occurs and produces electrons (e^-) and accompanied by the splitting of water into P_{680}*. Other energy is transformed into fluorescence and heat [5, 17, 23, 24, 27]. *Chl** conducts de-excitation by photochemistry, non-radiation heat dissipation, and chlorophyll fluorescence is then able to accept new photons, yet the process depends on the lifetime of *Chl* in the excited state [35, 36]. The released electrons pass through pheophytin to the primary electron acceptor Q_A and are ultimately transferred via a series of electron carriers to photosystem I, thereby generating ATP and reducing power NADPH to driving photosynthetic carbon fixation and respiratory carbon oxidation [5, 26]. Although classical *P–I* models have been widely used to fit the P_n–*I* curve for estimating photosynthetic performance and responses to environment changes for phytoplankton [18–22], many of them were not built based on the photosynthetic mechanism.

The exponential model established by Webb et al. [18] and model 1 are still applied extensively for phytoplankton [37–41] even though they lack photoinhibition function. For example, Ma et al. [40] indicated that the P_{nmax} calculated by model 1 for *M. aeruginosa* FACHB-905 and *M. aeruginosa* FACHB-469 were 253.92 ± 6.79 and 231.32 ± 6.40 μmol O_2 mg^{-1} Chl *a* h^{-1}, respectively, at 25 °C, yet the corresponding I_{sat} were only 92.71 ± 7.86 and 88.61 ± 3.22 μmol photons m^{-2} s^{-1}, respectively. Furthermore, the shape of their *P–I* curves did not appear to decline above I_{sat}. In present study, the results are as we expected that model 1 overestimated P_{nmax} and could not directly estimate the saturation irradiance (I_{sat}) because of it being an asymptotic function. The values of α, P_{nmax} and I_{sat} fitted by model 1 showed significant differences with those obtained by other models ($p < 0.05$); either P_{nmax} or I_{sat} were distinct from their measured data for seven species of phytoplankton (including *M. aeruginosa* FACHB-905), which suggests that an insufficient irradiance would be supplied to the cultivation if the I_{sat} obtained by model 1 was used as the optimal intensity of irradiance.

To describe the entire range of light levels of phytoplankton, Platt et al. [20, 21] proposed another empirical model with a photoinhibition function (model 2 in this study). Superficially, the P_n–*I* curves fitted by model 2 seem to be perfect as other studies [42, 43], but the value of P_s among the fitted results was notably higher than the value of P_{nmax} in seven phytoplankton species, specially, for *I. galbana*, *M. aeruginosa* and *S. obliquus* when $\beta > 0$ (Table 4). To calculate P_{nmax}, Eq. 7 must satisfy the condition of $\beta > 0$, otherwise it is unable to estimate directly P_{nmax} because model 2 will degenerate

Table 4 Comparison of P_s, P_{nmax} (μmol O_2 mg^{-1} Chl *a* h^{-1}) calculated by model 2 with measured value

Parameter	*I. galbana*	*D. salina*	*P. subcordiformis*	*M. aeruginosa*	*M. wesenbergii*	*S. obliquus*	*Chlorococcum* sp.
P_s ($\beta=0$)	135.44 ± 6.59	144.28 ± 10.86	133.39 ± 6.73	328.48 ± 18.27	235.77 ± 3.70	311.42 ± 7.37	96.21 ± 5.71
P_s ($\beta>0$)	14,188.6 ± 13,735.8	196.08 ± 31.06	135.23 ± 7.45	1163.4 ± 615.5	415.53 ± 29.50	943.8 ± 282.4	107.02 ± 5.53
P_{nmax}	97.45 ± 3.02	113.73 ± 6.24	94.64 ± 6.65	290.74 ± 15.09	195.32 ± 1.50	268.80 ± 5.21	75.25 ± 3.79
Observations	≈94	≈119	≈100	≈290	≈200	≈267	≈75

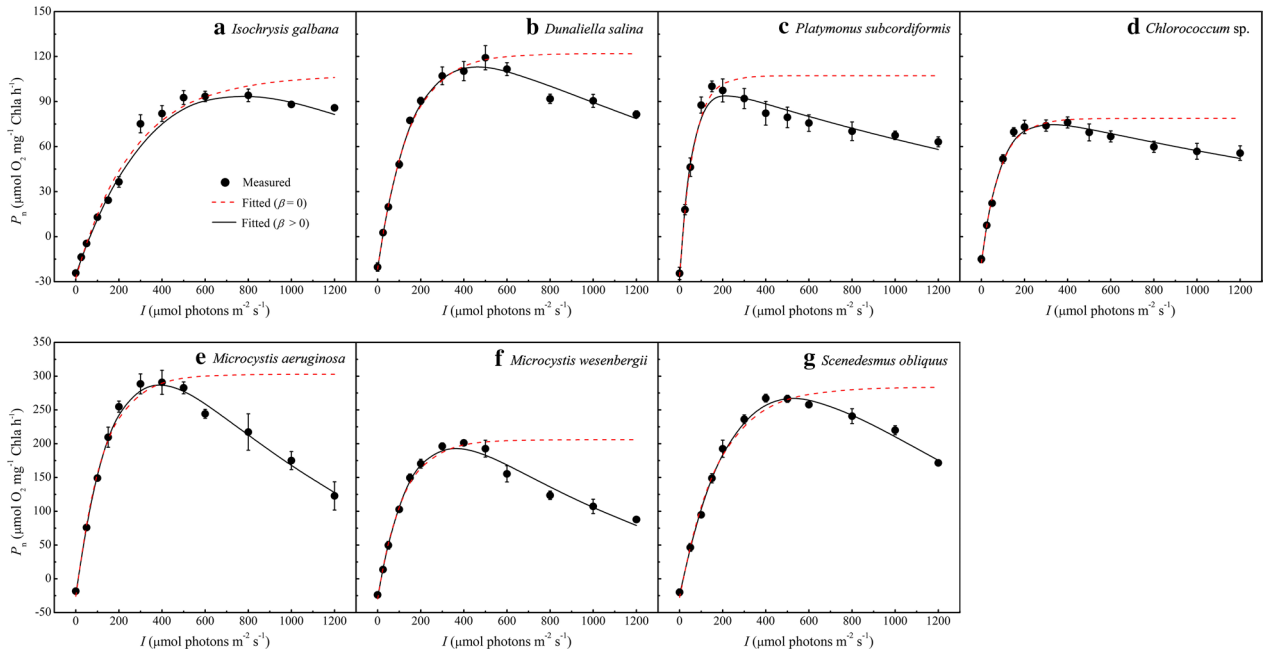

Fig. 5 The P_n–I curves produced by the model 2 at $\beta=0$ and $\beta>0$

into an exponential function without an extreme value when $\beta=0$, where there was no photoinhibition, and the fitting curves were similar to model 1 (Fig. 5). This reveals a clear disagreement with the definition of P_s that characterizes the output of dark reactions of photosynthesis in model 2. The analytic solution of I_c cannot be directly obtained by Eq. 5. To obtain I_c, the Kok effect must be ignored. However, the Kok effect was widespread observed in phytoplankton [33]. Currently, most researchers ignore these problems when they use model 2 to investigate and fit the P_n–I curves of phytoplankton [1, 43–45]. Therefore, model 2 may be treated carefully in explaining biological implication of P_s and estimating photosynthetic parameters.

Compared with previous models, model 3 is no longer just a mathematical equation describing the dependence of the photosynthetic rate on irradiance intensity. Its foundation is an assumption of "photosynthetic factories" (PSF) on physiological mechanisms proposed by Crill [46]. A PSF that is regarded as a combination of photosystem I (PSI) and PSII conducts one unit of light to generate one unit of photosynthetic product. And Eilers and Peeters assumed that the process of photosynthesis is modeled by changes of the states of PSF from the resting state to the activated and inhibited state [17, 22]. Model 3 yielded a good-fitting curve for the P_n–I data of all phytoplankton species in this study, and the returned values for P_{nmax}, I_c, and R_d were close to their measured values, except for I_{sat}, which showed a large deviation ($p<0.05$). Meanwhile, Fig. 1c shows that the I_{sat} of curve did not change with the value of β. This may be because the model neglects the detail process of the capture of solar energy, energy transfer process, and electron transport from PSII to Cytb6f and then to PSI.

Although differences between higher plants and phytoplankton are observed in photosynthetic antenna system and photosynthetic components [10, 16], in present study the P_n–I curves of all phytoplankton species fitted by model 4 were good and the returned values were also close to the measured data. This reveals

that model 4 for higher plants is applicable for phytoplankton. Acquiring an accurate and optimal parameter for irradiance intensity is essential to achieve high biomass of phytoplankton in production. Irradiance is rapidly attenuated during high-cell density cultivation of phytoplankton [14, 27]. Variation in the pigment composition of light harvesting complexes with irradiance intensity has been observed in most species of phytoplankton [4, 5]. Irradiance intensity also regulates the accumulation of triacylglycerols and carbohydrates [6, 7]. Note that obtained I_{sat} by model 4 was closer to the measured value than other three models. The differences between the returned values for P_{nmax}, I_c, and R_d by model 4 and their measured values were slightly larger than those by model 3, without significant differences ($p > 0.05$). For model 3 and model 4 with the same four parameters, they can be regarded as a semi-mechanistic model and mechanistic model in describing P_n–I curve, respectively. The former mainly characterizes and simulates P_n–I curves of phytoplankton, the latter mainly focuses on photosynthetic performance of photosynthetic organisms. In addition, the biological significance of parameters in model 3 is implicit except for γ. On the contrary, the biological significance of four parameters in model 4 is distinct. Consequently, model 4 may provide an alternative method in study photosynthetic characteristics of phytoplankton. The fitting curves by model 4 for *P. subcordiformis*, *M. aeruginosa*, *M. wesenbergii*, and *Chlorococcum* sp. exhibited some deviations under low intensity of irradiance, likely because the model targeted higher plants, which showed higher light dependence than phytoplankton.

In meso- and eutrophic water bodies, irradiance or temperature is a key factor affecting changes of phytoplankton community composition, especially for those that become the dominant population between cyanobacteria and green algae [47]. The results of this study explicitly demonstrate that *M. aeruginosa* and *M. wesenbergii* had high intrinsic quantum efficiency (α), while their Chl *a* content per cell was lower than that of both *S. obliquus* and *Chlorococcum* sp., indicating the efficient light harvesting and use for *M. aeruginosa* and *M. wesenbergii* because the intrinsic quantum yield represents the numbers of photosynthetic electrons required to assimilate one CO_2 molecule [8]. In addition, almost two times less α than both *S. obliquus* and *Chlorococcum* sp., and the largest P_{nmax} were found in *M. aeruginosa*. However, *M. aeruginosa* is the main contributor of notorious bloom-forming cyanobacteria in global freshwater bodies, such as Dianchi Lake in China [48]. These results reveal the underlying physiological basis of photosynthesis of *Microcystis* with lower "critical light intensity", and provide important insights into the management and control of cyanobacteria in changing lakes and estuarine waters.

I. galbana and *D. salina* are applied world-wide to generate biofuels due to their rich lipids (lipid levels between 23 and 55% by weight of dry biomass), and they are also commonly cultivated with *P. subcordiformis* (lipid levels between 20% and 30% by weight of dry biomass) for aquaculture in China, Japan, Australia, and southeast Asia [14, 49]. To meet nutritional requirements, mixed cultures of two or more species of phytoplankton are often fed to larvae in seed farming of aquatic products [50]. It is critical that the photosynthetic productivity of each strain reach as high as possible during production. The comparison revealed that, although the P_{nmax} lay between *I. galbana* and *P. subcordiformis*, other photosynthetic characteristic parameters showed great differences. The smallest α and highest I_c were found in *I. galbana*, which meant a low efficiency of light capture and use for *I. galbana*. In contrast, the largest α and lowest I_{sat} and I_c were in *P. subcordiformis*, although it possesses lower Chl *a* content per cell compared to *D. salina*. Consequently, the ranking of light-dependence in descending order was *P. subcordiformis*, *D. salina*, and *I. galbana*. Under co-culture conditions, a gradient of irradiance from low to mid to high can be supplied in one photoperiod.

Conclusions

Our study showed that significant differences were found between the returned values to photosynthetic characteristics by models 1, 2 and 3, some parameters (e.g., I_{sat}) were distinctly different to the measured data. Model 4 for higher plants reproduced the irradiance response trends of photosynthesis well, was applicable for phytoplankton, but more studies are required to investigate its flexibility and reusability. Differences in photosynthetic performance were observed among phytoplankton species. *P. subcordiformis* showed higher light-dependence than *D. salina* and *I. galbana*, while *M. aeruginosa* and *M. wesenbergii* exhibited more efficient light use than *S. obliquus* and *Chlorococcum* sp. These findings could contribute to a better understanding of structure changes of phytoplankton communities in the aquatic ecosystem, especially in those eutrophic lakes and estuaries.

Abbreviations

PSI: Photosystem I; PSII: Photosystem II; ROS: Reactive oxygen species; *P–I*: Response of photosynthesis to irradiance; PSF: Photosynthetic factories; Chl *a*: Chlorophyll *a*; *I*, μmol photons m^{-2} s^{-1}: Irradiance intensity; P_n, μmol O_2 mg^{-1} Cha h^{-1}: Net photosynthetic rate at irradiance *I*; P_{nmax}, μmol O_2 mg^{-1} Cha h^{-1}: Maximum net photosynthetic rate; I_{sat}, μmol photons m^{-2} s^{-1}: Saturation irradiance; *α*, μmol O_2 mg^{-1} Cha h^{-1}/μmol photons m^{-2} s^{-1}: Light-limited initial slope of P_n–*I* curve; I_c, μmol photons m^{-2} s^{-1}: Light compensation point; R_d, μmol O_2 mg^{-1} Cha h^{-1}: Dark respiration rate; R^2: Adjusted coefficient of determination; P_n', μmol O_2 μmol photons $^{-1}$: Photosynthetic quantum efficiency; P_n'–*I*: Response of photosynthetic quantum efficiency to irradiance;

P_s: Parameter reflecting the maximum, potential, light-saturated, rate of photosynthesis in model 2; *Chl*: Photosynthetic pigment molecules; *Chl**: Excited state of photosynthetic pigment molecules.

Acknowledgements
We thank the National Science Foundation for financial support of this research. We gratefully acknowledge the anonymous reviewers for their constructive and positive comments. I also would like to express my deepest thanks to my family in Ji'an city, China, for their love and support.

Authors' contributions
XLY conceived the original study, wrote the paper. XLY and LHL performed the experiment and data analysis. XYW and ZKY conducted the isolation and identification of marine phytoplankton. SBW and ZPY supervised the experiment and editing of paper. All authors read and approved the manuscript.

Funding
This research was supported by the Natural Science Foundation of China (Grant Nos. 31960054, 31560069).

Availability of data and materials
The datasets supporting the conclusions of this article are included within the article.

Ethics approval and consent to participate
Not applicable.

Consent for publication
All authors consented to the publication of this work.

Competing interests
The authors declare no competing interests.

Received: 18 December 2019 Accepted: 9 February 2020
Published online: 26 February 2020

References

1. Bouman HA, Platt T, Doblin M, Figueiras FG, Sathyendranath S (2018) Photosynthesis-irradiance parameters of marine phytoplankton: synthesis of a global data set. Earth Syst Sci Data 10:251–266
2. Novak T, Godrijan J, Pfannkuchen DM, Djakovac T, Medic N, Ivancic I, Mlakar M, Gasparovic B (2019) Global warming and oligotrophication lead to increased lipid production in marine phytoplankton. Sci Total Environ 668:171–183
3. Kwiatkowski L, Aumont O, Bopp L, Ciais P (2018) The impact of variable phytoplankton stoichiometry on projections of primary production, food quality, and carbon uptake in the global ocean. Global Biogeochem Cycles 32:516–528
4. Kieselbach T, Cheregi O, Green BR, Funk C (2018) Proteomic analysis of the phycobiliprotein antenna of the cryptophyte alga *Guillardia theta* cultured under different light intensities. Photosynth Res 135:149–163
5. Pathak J, Ahmed H, Singh PR, Singh SP, Häder D-P, Sinha RP (2019) Mechanisms of photoprotection in cyanobacteria. In: Mishra AK, Tiwari DN, Rai AN (eds) Cyanobacteria: From basic science to applications. Academic Press, London, pp 145–171
6. Ho S-H, Ye X, Hasunuma T, Chang J-S, Kondo A (2014) Perspectives on engineering strategies for improving biofuel production from microalgae-a critical review. Biotechnol Adv 32:1448–1459
7. Huete-Ortega M, Okurowska K, Kapoore RV, Johnson MP, Gilmour DJ, Vaidyanathan S (2018) Effect of ammonium and high light intensity on the accumulation of lipids in *Nannochloropsis oceanica* (CCAP 849/10) and *Phaeodactylum tricornutum* (CCAP 1055/1). Biotechnol Biofuels 11:60
8. Wang HT, Meng YY, Cao XP, Ai JN, Zhou JN, Xue S, Wang WL (2015) Coordinated response of photosynthesis, carbon assimilation, and triacylglycerol accumulation to nitrogen starvation in the marine microalgae *Isochrysis zhangjiangensis* (Haptophyta). Biores Technol 177:282–288
9. Geider RJ, MacIntyre HL (2001) Physiology and biochemistry of photosynthesis and algal carbon acquisition. In: Williams PLB, Thomas DN, Reynolds CS (eds) Microalgae productivity: carbon assimilation in marine and freshwater ecosystems. Blackwell Science, Oxford, pp 44–77
10. Pachiappan P, Santhanam P, Begum A, Prasath BB (2019) An Introduction to Plankton. In: Santhanam P, Begum A, Pachiappan P (eds) Basic and applied microalgae biology. Springer, Berlin, pp 1–24
11. Stephenson PG, Moore CM, Terry MJ, Zubkov MV, Bibby TS (2011) Improving photosynthesis for algal biofuels: toward a green revolution. Trends Biotechnol 29:615–623
12. Racault M-F, Raitsos DE, Berumen ML, Brewin RJ, Platt T, Sathyendranath S, Hoteit I (2015) Phytoplankton phenology indices in coral reef ecosystems: application to ocean-color observations in the Red Sea. Remote Sens Environ 160:222–234
13. Burson A, Stomp M, Greenwell E, Grosse J, Huisman J (2018) Competition for nutrients and light: testing advances in resource competition with a natural phytoplankton community. Ecology 99:1108–1118
14. Borowitzka M (2019) Commercial-scale production of microalgae for bioproducts. In: La Barre S, Bates SS (eds) Blue biotechnology—production and use of marine molecules. Wiley, New Jersey, pp 33–65
15. Ogbonna JC, Tanaka H (2000) Light requirement and photosynthetic cell cultivation–development of processes for efficient light utilization in photobioreactors. J Appl Phycol 12:207–218
16. Abu-Ghosh S, Dubinsky Z, Banet G, Iluz D (2018) Optimizing photon dose and frequency to enhance lipid productivity of thermophilic algae for biofuel production. Biores Technol 260:374–379
17. Darvehei P, Bahri PA, Moheimani NR (2018) Model development for the growth of microalgae: a review. Renew Sustain Energy Rev 97:233–258
18. Webb WL, Newton M, Starr D (1974) Carbon dioxide exchange of *Alnus rubra*. A mathematical model. Oecologia 17:281–291
19. Platt T, Jassby AD (1976) The relationship between photosynthesis and light for natural assemblages of coastal marine phytoplankton. J Phycol 12:421–430
20. Platt T, Gallegos C, Harrison WG (1980) Photoinhibition of photosynthesis in natural assemblages of marine phytoplankton. J Mar Res 38:687–701
21. Platt T, Harrison WG, Irwin B, Horne EP, Gallegos CL (1982) Photosynthesis and photoadaptation of marine phytoplankton in the Arctic. Deep Sea Res Part A Oceanogr Res Papers 29:1159–1170
22. Eilers PHC, Peeters JCH (1988) A model for the relationship between light intensity and the rate of photosynthesis in phytoplankton. Ecol Model 42:199–215
23. Han BP (2001) Photosynthesis–irradiance response at physiological level: a mechanistic model. J Theor Biol 213:121–127
24. Rubio FC, Camacho FG, Sevilla JM, Chisti Y, Grima EM (2003) A mechanistic model of photosynthesis in microalgae. Biotechnol Bioeng 81:459–473
25. Bernard O, Remond B (2012) Validation of a simple model accounting for light and temperature effect on microalgal growth. Biores Technol 123:520–527
26. Garcia-Camacho F, Sanchez-Miron A, Molina-Grima E, Camacho-Rubio F, Merchuck JC (2012) A mechanistic model of photosynthesis in microalgae including photoacclimation dynamics. J Theor Biol 304:1–15
27. Bechet Q, Chambonniere P, Shilton A, Guizard G, Guieysse B (2015) Algal productivity modeling: a step toward accurate assessments of full-scale algal cultivation. Biotechnol Bioeng 112:987–996
28. Jayaraman SK, Rhinehart RR (2015) Modeling and optimization of algae growth. Ind Eng Chem Res 54:8063–8071
29. Ye ZP, Suggett DJ, Robakowski P, Kang HJ (2013) A mechanistic model for the photosynthesis-light response based on the photosynthetic electron transport of photosystem II in C3 and C4 species. New Phytol 199:110–120
30. Li X, Cai J, Liu F, Dai T, Cao W, Jiang D (2014) Exogenous abscisic acid application during grain filling in winter wheat improves cold tolerance of offspring's seedlings. J Agronomy Crop Sci 200:467–478
31. Wu A, Song Y, Van Oosterom EJ, Hammer GL (2016) Connecting biochemical photosynthesis models with crop models to support crop improvement. Front Plant Sci 7:1518
32. Jeffrey SW, Humphrey GF (1975) New spectrophotometric equations for determining chlorophylls *a*, *b*, *c*1 and *c*2 in higher plants, algae and natural phytoplankton. Biochemie Und Physiol Der Pflanzen 167:191–194
33. Kok B (1948) A critical consideration of the quantum yield of *Chlorella* photosynthesis. Enzymologia 13:1–56

34. Posada D, Buckley TR (2004) Model selection and model averaging in phylogenetics: advantages of Akaike information criterion and bayesian approaches over likelihood ratio tests. Syst Biol 53:793–808
35. Ye ZP (2012) Nonlinear optical absorption of photosynthetic pigment molecules in leaves. Photosynth Res 112:31–37
36. Ooms MD, Dinh CT, Sargent EH, Sinton D (2016) Photon management for augmented photosynthesis. Nat Commun 7:12699
37. Chen B, Zou D, Ma Z, Yu P, Wu M (2019) Effects of light intensity on the photosynthetic responses of *Sargassum fusiforme* seedlings to future CO_2 rising. Aquact Res 50:116–125
38. Hill EA, Chrisler WB, Beliaev AS, Bernstein HC (2017) A flexible microbial co-culture platform for simultaneous utilization of methane and carbon dioxide from gas feedstocks. Bioresour Technol 228:250–256
39. Kim M, Brodersen KE, Szabó M, Larkum AWD, Raven JA, Ralph PJ, Pernice M (2018) Low oxygen affects photophysiology and the level of expression of two-carbon metabolism genes in the seagrass *Zosterae*. Photosynth Res 136:147–160
40. Ma Z, Fang T, Thring RW, Li Y, Yu H, Zhou Q, Zhao M (2015) Toxic and non-toxic strains of *Microcystis aeruginosa* induce temperature dependent allelopathy toward growth and photosynthesis of *Chlorella vulgaris*. Harmful Algae 48:21–29
41. Park J, Dinh TB (2019) Contrasting effects of monochromatic LED lighting on growth, pigments and photosynthesis in the commercially important cyanobacterium *Arthrospira maxima*. Bioresour Technol 291:121846
42. Vu MTT, Douëtte C, Rayner TA, Thoisen C, SrL Nielsen, Hansen BW (2016) Optimization of photosynthesis, growth, and biochemical composition of the microalga *Rhodomonas salina*—an established diet for live feed copepods in aquaculture. J Appl Phycol 28:1485–1500
43. Stawiarski B, Buitenhuis ET, Fallens M (2018) The physiological response of seven strains of picophytoplankton to light, and its representation in a dynamic photosynthesis model. Limnol Oceanogr 63:S367–S380
44. Sutherland DL, Montemezzani V, Howard-Williams C, Turnbull MH, Broady PA, Craggs RJ (2015) Modifying the high rate algal pond light environment and its effects on light absorption and photosynthesis. Water Res 70:86–96
45. Jiang H, Zou D, Chen W, Yang Y (2017) The photosynthetic responses to stocking depth and algal mat density in the farmed seaweed *Gracilaria lemaneiformis* (Gracilariales, Rhodophyta). Environ Sci Pollut Res Int 24:25309–25314
46. Crill PA (1977) The photosynthesis-light curve: a simple analog model. J Theor Biol 64:503–516
47. Qian Y, Liu Z, Chen Y, Zhu D, Na L (2018) Modelling the impact of hydrodynamic turbulence on the competition between *Microcystis* and *Chlorella* for light. Ecol Model 370:50–58
48. Yang XL, Liu LH, Wang SB (2019) A strategy of high-efficient nitrogen removal by an ammonia-oxidizing bacterium consortium. Biores Technol 275:216–224
49. Chisti Y (2007) Biodiesel from microalgae. Biotechnol Adv 25:294–306
50. Ehteshami F, Romano N, Ramezani Fard E, Hoseinzadeh Sahafi H (2017) Effect of different dietary microalgae combinations on growth and survival of black-lip pearl oyster (*Pinctada margaritifera*) larvae and the feasibility of replacing microalgae with a dietary lipid emulsion. Aquact Nutr 23:671–680

Publisher's Note